analytical chemistry

Letter

pubs.acs.org/ac

Open-Channel Microfluidic Membrane Device for Long-Term FT-IR Spectromicroscopy of Live Adherent Cells

Kevin Loutherback, Liang Chen, and Hoi-Ying N. Holman*

Berkeley Synchrotron Infrared Structural Biology (BSISB) Program, Earth Sciences Division, Lawrence Berkeley National Laboratory, Berkeley, California 94720, United States

Supporting Information

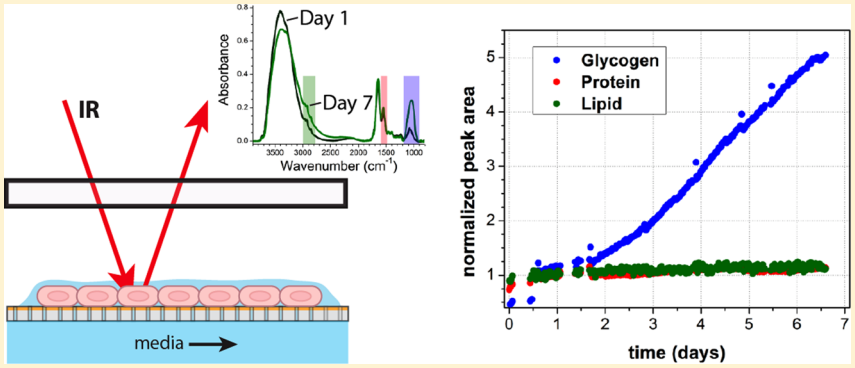

ABSTRACT: Spatially resolved infrared spectroscopy is a label-free and nondestructive analytical technique that can provide spatiotemporal information on functional groups in biomolecules of a sample by their characteristic vibrational modes. One difficulty in performing long-term FT-IR measurements on live cells is the competition between the strong IR absorption from water and the need to supply nutrients and remove waste. In this proof of principle study, we developed an open-channel membrane device that allows long-term continuous IR measurement of live, adherent mammalian cells. Composed of a gold-coated porous membrane between a feeding channel and a viewing chamber, it allows cells to be maintained on the upper membrane surface in a thin layer of fluid while media is replenished from the feeding channel below. Using this device, we monitored the spatiotemporal chemical changes in living colonies of PC12 cells under nerve growth factor (NGF) stimulation for up to 7 days using both conventional globar and high-resolution synchrotron radiation-based IR sources. We identified the primary chemical change cells undergo is an increase in glycogen that may be associated with secretion of glycoprotein to protect the cells from evaporative stress at the air−liquid interface. Analyzing the spectral maps with multivariate methods of hierarchical cluster analysis (HCA) and principal component analysis (PCA), we found that the cells at the boundary of the colony and in a localized region in the center of the colony tend to produce more glycogen and glycoprotein than cells located elsewhere in the colony and that the degree of spatial heterogeneity decreases with time. This method provides a promising approach for long-term live-cell spectromicroscopy on mammalian cell systems.

Spatially resolved infrared spectroscopy is a label-free[1] and nondestructive[2] analytical technique that can provide spatiotemporal chemical maps of functional groups in biomolecules of a sample by their characteristic vibrational modes.[3,4] It has been used extensively for tissue pathology[5,6] and is increasingly employed in studying the chemical response in live cells to environmental perturbations.[7−9] There is strong recent interest to use this technique for noninvasive study of live mammalian cell systems to gain insight into disease progression,[10−12] drug discovery,[13] cell regulation, and development.[14,15]

One challenge in performing FT-IR measurements on live cells is the competition between water film thickness and the need to supply nutrients and remove waste.[7,16] Absorption from water can quickly saturate the IR signal for thicknesses greater than about 10 μm, obscuring chemical bands associated with protein secondary structure (amide I) and membrane integrity (C−H). A common approach for live-cell study is to sandwich two IR-transparent windows between a thin spacer or patterned microstructures to form a closed chamber.[16−21] The problem with this approach for adherent mammalian cells is the small space requires frequent feeding that introduces shear stress, adversely affecting cell attachment and proliferation.[22] As a result, these devices have been limited to measurements of around 48 h for adherent mammalian cells. Attenuated total reflection (ATR)-FT-IR imaging is a promising approach that allows cells to be maintained in a thicker layer of water[23] but is limited to measuring only materials in close contact with the crystal by the penetration depth of the evanescent wave.[7,9]

Received: February 8, 2015
Accepted: April 17, 2015
Published: April 17, 2015

DOI: 10.1021/acs.analchem.5b00524
Anal. Chem. 2015, 87, 4601−4606

Synchrotron-radiation-FT-IR (SR-FT-IR) additionally allows probing the spatial variation in the chemical composition of single cells.[3,24] Using a broadband, high-brightness synchrotron source instead of the standard thermal source gives diffraction-limited spatial resolution with ~200 times increase in signal-to-noise ratio that allows single mammalian cells to be resolved. This superior resolution allows for identification of variable responses within a colony of cells that is unavailable using a globar source.

We developed an open channel device that allows long-term continuous IR measurement of live, adherent mammalian cells. Composed of a gold-coated porous membrane between a feeding channel and a viewing chamber, it allows continuous transflection measurement of live cells in a thin layer of liquid. Using this device, we monitored the spatiotemporal chemical changes in living colonies of PC12 cells for several days. We measured cells for 7 days with 30 min spacing using a globar illumination source and for 4.5 days with high-resolution mapping and synchrotron infrared (SIR) illumination with 45 min spacing. Using the globar source, we identified the primary chemical change cells undergo is increase in glycogen that may be associated with secretion of glycoproteins,[25] acting as a surfactant to protect the cells from evaporative stress at the air–liquid interface. Using the SIR data and hierarchical cluster analysis (HCA) to group cells with similar spectral features, we found that cells at the boundary of the colony and in a localized region in the center of the colony tend to produce more glycogen and glycoprotein than other cells in the colony. Principal component analysis (PCA) further showed the spatiotemporal evolution of the colony.

EXPERIMENTAL SECTION

Devices shown in Figure 1 are made of a gold-coated polyester membrane fixed between two layers of milled polycarbonate. Track-etched polyester membranes with 400 nm pores are extracted from Transwell (Corning) membrane inserts after being coated with 15 nm of gold via e-beam evaporation. The pore size is small enough that the coated-membrane surface reflects IR illumination uniformly without any noticeable scattering. SIR measurements in Figure S1 in the Supporting Information show that the reflectivity of the bare membrane is 97 ± 1% compared to a mirrIR (Kevley Technologies) slide over the spectral range of 800–4000 cm^{-1} under various conditions. The upper and lower pieces are fabricated out of polycarbonate sheets using a Roland DG MDX-20 milling machine. The lower piece has a 2 mm deep channel that increases linearly in width from 2 mm at the inlet/outlet to 6 mm below the membrane milled into a 3 mm thick polycarbonate sheet. The upper piece is composed of a 6 mm circular viewing window that forms the cell chamber when sealed against the membrane and inlet/outlet ports to connect to the lower chamber milled into a 1 mm polycarbonate sheet. The device is assembled by gluing the membrane between upper and lower pieces using medical-grade epoxy (Loctite M-31CL) and curing at 80 °C for 1 h.

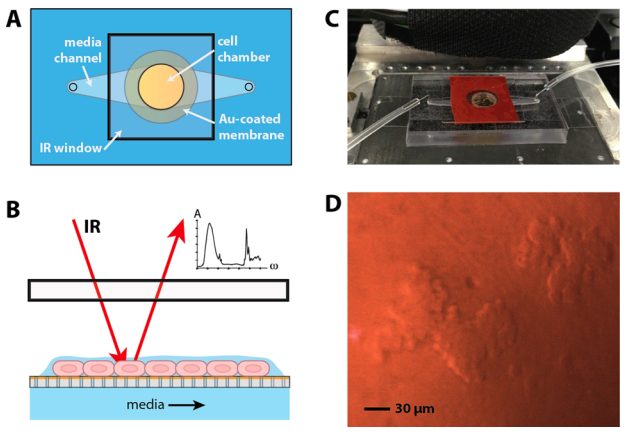

Figure 1. Microfluidic membrane device schematic: (A) Device is composed of a gold-coated, porous membrane sandwiched between a media channel and a cell chamber milled out of polycarbonate. Cell chamber is sealed with an IR-transparent window. (B) Cells are maintained in thin film of fluid that allows probing with IR light. Nutrients are supplied from the media channel below the membrane. (C) Device mounted on microscope with heated stage and objective. (D) Bright-field image of PC12 cell colonies on membrane.

After coating both sides of the membrane and the lower channel with collagen, the lower channel of the device was wet with CO_2-independent media supplemented with 25 ng/mL NGF. PC12 cells are a neuronal development model cell line that differentiates into neuron-like cells when treated with NGF.[26] Previous studies of this system at isolated time points showed increasing protein phosphorylation associated with differentiation using FT-IR spectromicroscopy.[15] Approximately 20 000 cells were seeded onto the membrane in 20 μL of media. Cells were incubated at 37 °C for 2 h to attach to the membrane surface before excess media was aspirated from the upper chamber. The chamber was then sealed with a 0.3 mm thick CaF_2 window pressed onto a rubber gasket to maintain a humid environment while allowing IR measurements. Continuous flow of media was maintained in the lower channel at a rate of 100 nL/min via syringe pump, and the device was mounted on a microscope stage heated to 36 °C. Cells were observed with a 15× reflachromat objective heated to 38 °C to limit condensation on the window. Cell viability was tested after 3 days in a control experiment where cells were grown on a membrane device with identical experimental conditions in a 37 °C incubator. Trypan blue vital staining shown in Figure S3 in the Supporting Information indicates that the cells remain viable.

Continuous real-time measurements of live PC12 cells were performed using both globar and synchrotron-radiation infrared illumination at Beamline 1.4.3 of the Advanced Light Source at Lawrence Berkeley National Laboratory. Limited beamtime availability necessitated performing initial experiments using a globar source for 7 days followed by 4 days of beamtime with SIR illumination. In the first experiment, globar illumination was used to take 274 spectral maps of a colony of PC12 cells using a 4 × 4 grid with 100 μm step size and 30 min spacing for 1 week. In the second experiment, SIR illumination was used to take 76 spectral maps of a colony of PC12 cells using a 21 × 20 grid with 10 μm step size and 45 min spacing for 4.5 days. IR spectra were obtained using transflection measurement mode between 4000 and 800 cm^{-1} at 4 cm^{-1} spectral resolution and averaged with 16 coadded scans. We do not expect electric field standing wave effects[27,28] to be significant because of variation in sample thickness, illumination coherence, and range of incidence angles from the 15× objective.[29] After measurement, all spectra were baseline corrected without the need for bulk-water subtraction. Synchrotron mapping data were filtered by thresholding the amide II band (1580–1480 cm^{-1}) intensity at

DOI: 10.1021/acs.analchem.5b00524
Anal. Chem. 2015, 87, 4601–4606

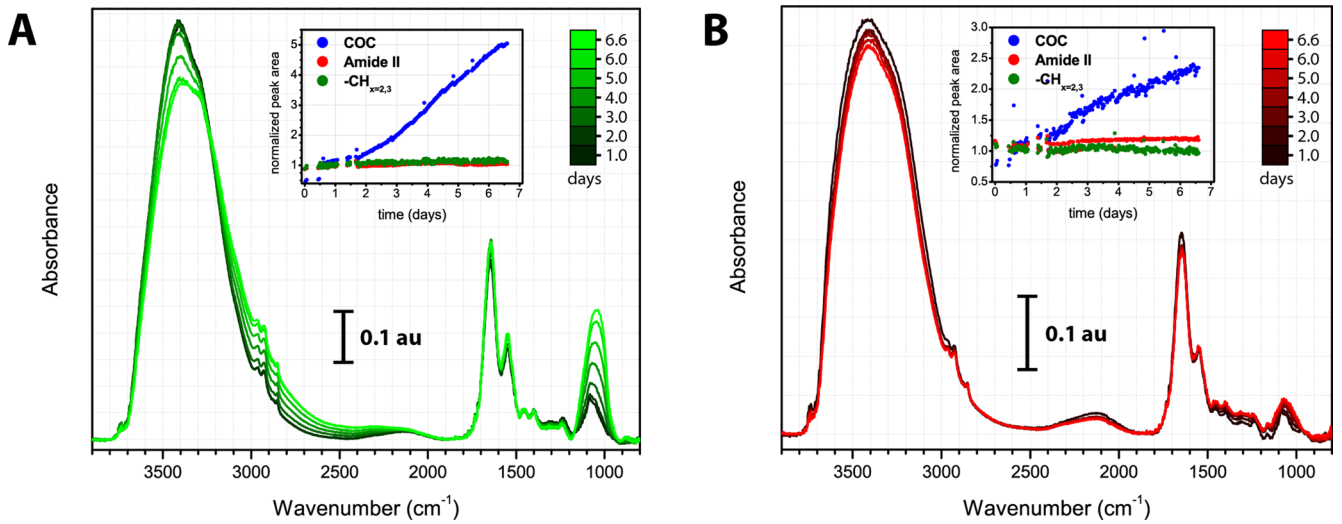

Figure 2. Multiday measurement of cells at two locations using a globar IR source. The spectral progression of a colony of PC12 cells is shown for the center (A) and edge (B). Vertical scale is in absorbance units (au). Insets show the peak area of glycogen and glycoprotein (1190−930 cm^{-1}), amide II (1580−1480 cm^{-1}), and $-CH_{2,3}$ (3000−2800 cm^{-1}) bands normalized to t = 0.

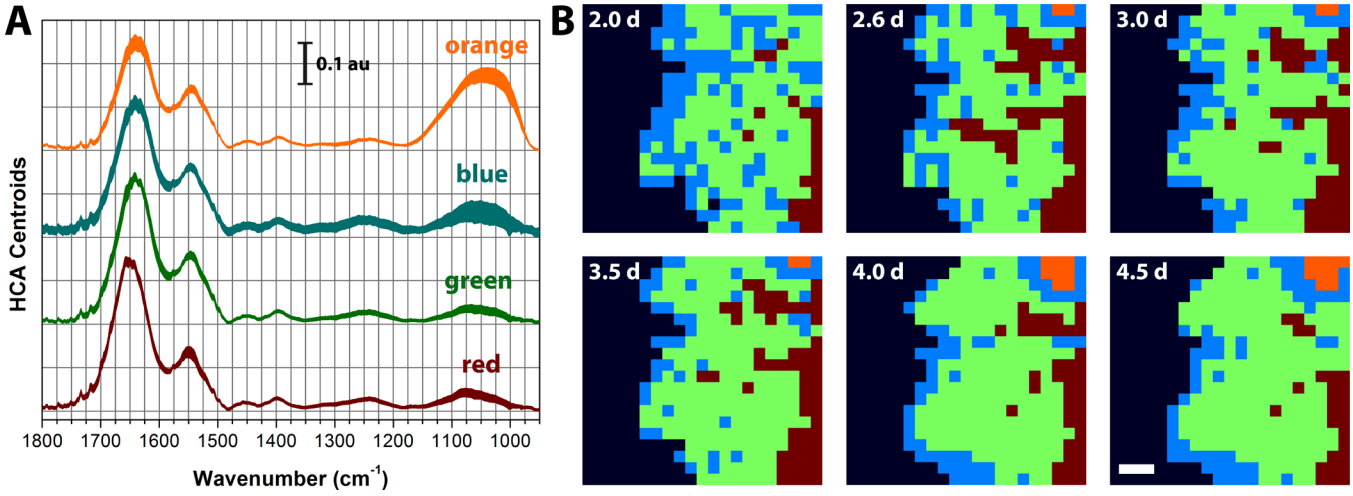

Figure 3. Multiday synchrotron IR measurement of cells: hierarchical cluster analysis (HCA). (A) Cluster centroids of the 1800−950 cm^{-1} region for all spatial and time points with four groups. The HCA cluster centroids are plotted offset on a common scale with area filled between 1.0 standard deviation of the mean. Vertical scale is in absorbance units (au). (B) Cluster maps for four time points between 2.0 and 4.5 days of a colony of PC12 cells with each pixel colored by the HCA cluster assignment. Empty pixels were filtered from the data analysis and colored dark blue. Scalebar is 30 μm.

the mean value minus 1.0 standard deviation of all points to exclude blank pixels in each map.

RESULTS AND DISCUSSION

Using this device, we were able to observe the spatiotemporal changes in chemical composition of a colony of PC12 cells over a period of 7 days. The spectral progression is shown for two locations in the 4 × 4 globar map in Figure 2 for the center (A) and edge (B) of the colony. The inset shows the peak area of the spectral regions between 1190 and 930 cm^{-1} dominated by the vibrational modes of C−O−C, C−O−P, and C−O stretching of various glucose storage molecules called glycogen and glycoproteins; between 1580 and 1480 cm^{-1} covering the protein amide II band; and between 3000 and 2800 cm^{-1} covering the C−H vibrations of the $-CH_3$ and $>CH_2$ functional groups of fatty acid chains. The changes in spectral intensity with respect to time shown in Figure 2 insets indicate that the cells remained metabolically active during the 7 day measurement window. The dominant spectral changes in the pixel associated with the center of the colony are a 5× increase in the 1190−930 cm^{-1} region associated with C−O−C, C−O−P, and C−O stretching in glycogen and glycoprotein[30] and a redshift in the −OH band (3600−3000 cm^{-1}) that corresponds to changing structure of cellular water.[31] The pixel at the edge of the colony has an increase in the glycogen and glycoprotein band intensity of about 2.5× over the measurement period. We interpret that the spectral changes could resemble a response to evaporative stress from growing at an air−liquid interface in contrast to those of protein phosphorylation previously observed for differentiating cells. Our interpretation is based on the lack of neurite outgrowth that is characteristic of PC12 differentiation upon treatment with NGF and that an additional pathway activated by treatment with NGF is the excretion of glycoproteins,[25] a constituent component of mucus that is known to provide protection against evaporative stress.[32]

DOI: 10.1021/acs.analchem.5b00524
Anal. Chem. 2015, 87, 4601−4606

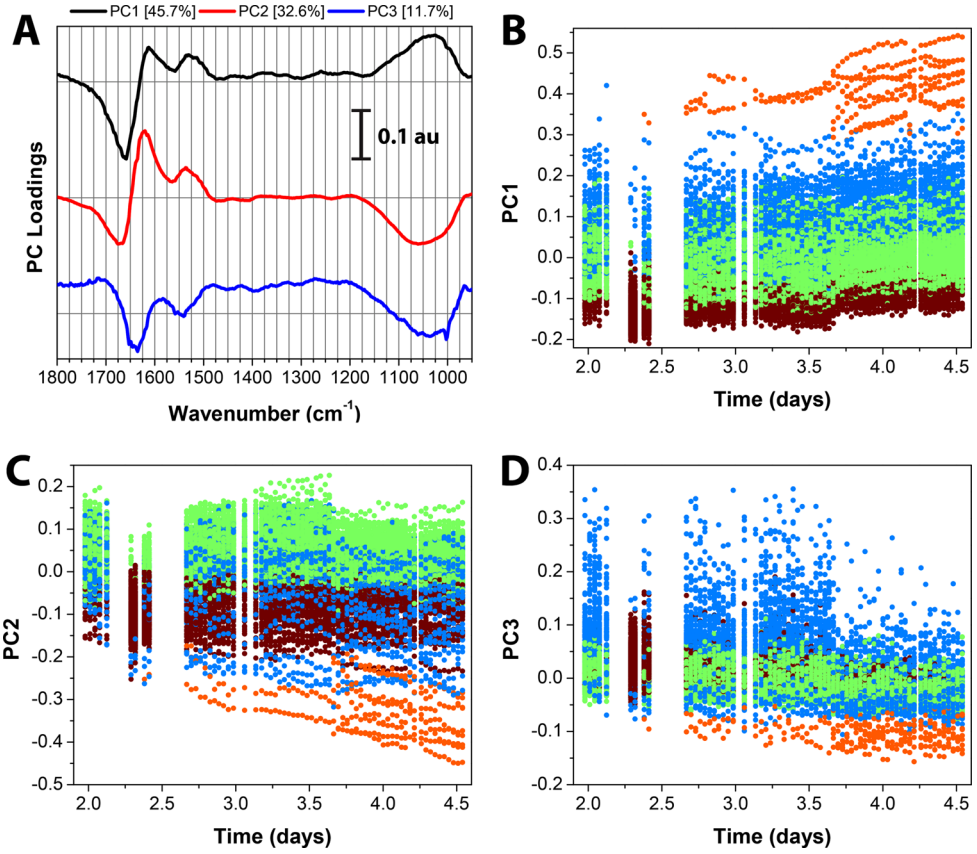

Figure 4. Time evolution of principal component score as indicator of chemical changes in multiday synchrotron measurement. (A) PC vectors for the region of 1800−950 cm^{-1} for all spatial and time points offset on a common scale. Vertical scale is in absorbance units (au). (B−D) PC scores versus time for each pixel on all maps with color assignment from HCA in Figure 3. Note that HCA group assignment for individual pixels can change between time points.

In a second experiment, we demonstrate that we were able to gain a more in-depth understanding of the spatiotemporal dynamics of the system using a high-resolution SIR source. Here, we used the same environmental conditions as above but monitored the chemical dynamics of a colony of cells between 2.0 and 4.5 days after loading. A hierarchical cluster analysis (HCA) of the 1800−950 cm^{-1} region for all spatial and time points was performed and the resultant four cluster centroids are shown in Figure 3A along with cluster maps for six time points between 2.0 and 4.5 days in Figure 3B. The maps show part of a colony of PC12 cells that continues out of the right of the frame with each pixel labeled with the HCA cluster assignment. The HCA cluster centroids are plotted with area filled between 1.0 standard deviation of the mean. We have additionally plotted the mean spectra for each cluster at the selected time points in Figure S2 in the Supporting Information.

The HCA spectral clusters are distinguished primarily by the intensity of the glycogen peak and the location of the amide I peak, which is particularly sensitive to protein secondary structure. The red cluster has an amide I peak location centered around 1653 cm^{-1} and lower glycogen and can be found primarily in the center of the colony with patches near the colony edge that recede with time. Trypan blue vital staining shown in Figure S3 in the Supporting Information indicates that cells away from the colony edges remain viable. As a result, we assign this group to healthy cells. The majority of the pixels are assigned to the green cluster, which has a low amount of glycogen and amide I peak shifted to 1641 cm^{-1}, indicating increased prevalence of beta-sheet configuration of protein.[33] While the green cluster is interspersed with blue and red clusters in the earlier time points, it occupies most of the intermediate area between the edge and center of the colony by the fourth day.

While the globar data may suggest that the glycogen intensity increases are localized primarily in the center of a colony, the higher resolution available using the synchrotron source (100 μm vs 10 μm pixel size) shows that the high-glycogen intensity areas are localized in two distinct areas: at the edges of the colony (blue group) and a small region in the center of the colony (orange group). The blue cluster is characterized by stronger glycogen intensity and amide I peak at 1641 cm^{-1}. The blue cluster is initially distributed throughout the map but is primarily concentrated at the edge of the colony as time progresses. This distribution supports the interpretation that increase of glycogen and glycoprotein is associated with the higher surface stress at the colony edges. The orange cluster is characterized by a broad glycogen peak at 1038 cm^{-1} and amide I peak at 1641 cm^{-1}. This group is very similar to what we saw in the globar experiment where there is strong glycogen production away from the colony edge. The physiological interpretation for this is uncertain, but this region continues to produce high amounts of glycogen and glycoprotein and increases in size throughout the experiment. In both cases, we observed that higher glycogen and glycoprotein production is associated with colony boundaries and a localized region in the center of the colony and that the spatial distribution of clusters while initially dispersive becomes more partitioned with time.

DOI: 10.1021/acs.analchem.5b00524
Anal. Chem. 2015, 87, 4601−4606

To examine the spatiotemporal chemical evolution of the colony, we performed a principal component analysis of all pixels over time. All spatial and temporal spectra were pooled and a principal component analysis was performed in the region of 1800−950 cm^{-1}. The principal component vector loadings in Figure 4A indicate the major bands with correlational changes among those bands that contribute to differentiate the spectra in the four HCA clusters. Ten principal components were needed to account for 97% of the spectral variation across all spatiotemporal data points while the first three principal components account for 90% of the variation. The main features of PC1, which explains 45.7% of the total variance are a glycogen peak in the 900−1200 cm^{-1} region with maximum at 1025 cm^{-1}, a protein (amide II) peak with maximum at 1540 cm^{-1}, and a zero-crossing at 1625 cm^{-1} in the amide I region which is interpreted as redshift toward more β-sheet protein structure. PC2 contains a similar structure but has a glycogen peak centered at 1060 cm^{-1} that is anticorrelated with a redshift in the amide I region with a zero crossing at 1650 cm^{-1}. PC3 contains a glycogen peak with a maximum at 1030 cm^{-1} correlated with an amide I peak with a maximum at 1630 cm^{-1}.

Chemical changes in the colony can be visualized by the temporal shifts in the mean and spread of the principal component scores between and within each HCA cluster. The principal component scores of each pixel for each time point are shown in Figure 4B−D with color assignment consistent with HCA clusters in Figure 3A. The plot indicates a tendency of increasing PC1 scores across all groups, with the orange cluster (strong glycogen) having the highest score followed by the blue cluster (medium glycogen), green cluster (weak glycogen), and red cluster (cells in the center of the colony). This ordering (excluding the orange cluster) follows the spatial ordering from the edge to interior of the colony in the map and probably reflects the primary features of glycogen and glycoprotein production. The orange cluster shows increasing PC1 scores and decreasing PC2 scores that correspond to increasing glycogen intensity with time. The green and red clusters did not show much change except for a slight increase in PC1 which can be interpreted as glycogen and glycoprotein secretion. The behavior of the blue cluster is the most varied. While showing high and increasing PC1 scores, it had a large spread and slight decrease in PC2 scores, which has a similar loading to PC1 except the opposing sign of coefficients in the glycogen region. The lower group of the bimodal distribution in blue cluster in PC3 score vs time is likely due to assignment of pixels near the boundary of the high glycogen region (orange cluster) as medium glycogen (blue cluster). However, the overall trend is decreasing scores with time, with a large variance in the upper group diminishing after 3.5 days. The HCA group assignment can change for the same pixel in different time points, so it may be the case that the decrease in variance indicates reclassification of pixels from the blue cluster (medium glycogen) to the green cluster (low glycogen group), which is also indicated in HCA cluster maps. The synchrotron mapping data is invaluable in allowing us to differentiate the responses at a functional group level of different regions of the colony to the experimental conditions. We interpret these results as an indicator that the cells respond to the liquid−air interface in the device by secreting glycogen and glycoprotein and that the distribution is concentrated at a localized region in the center of the colony and the edges of the colony where the evaporative stresses are highest.

CONCLUSION

This work demonstrates continuous FT-IR spectromicroscopy measurements of live adherent mammalian cells for up to 1 week with an open channel microfluidic device. This device allows long-term continuous high-resolution IR chemical imaging of live adherent mammalian cells. On the basis of a gold-coated porous plastic membrane, we used this device to spectroscopically measure living colonies of PC12 cells for several days using globar and synchrotron-based IR illumination. We observed increased signal intensity of glycogen that may be associated with secretion of glycoprotein to help cells hold moisture while growing at an air−liquid interface. Applying a combination of hierarchical cluster analysis and principal component analysis to the SIR mapping data, we were able to observe that the distribution of high glycogen and glycoprotein content regions is varied and biased toward the edges of the cell colonies where surface stresses are greatest and a localized region in the center of the colony. Furthermore, the spatial distribution of chemically similar clusters at a functional group level becomes more localized with time. The induction of a protective response rather than differentiation in PC12 cells suggest that future applications with this device are best suited toward cell lines that typically grow at an air-to-liquid interface such as epithelial cell lines derived from lung, skin, or eyes.

ASSOCIATED CONTENT

Supporting Information

Gold-coated membrane reflectivity (Figure S1); mean spectra of HCA clusters at various time points (Figure S2); and trypan blue vital stain of PC12 cells after 3 days on membrane (Figure S3). This material is available free of charge via the Internet at http://pubs.acs.org.

AUTHOR INFORMATION

Corresponding Author

*E-mail: hyholman@lbl.gov.

Notes

The authors declare no competing financial interest.

ACKNOWLEDGMENTS

This work was performed under the Berkeley Synchrotron Infrared Structural Biology (BSISB) Program funded by the U.S. Department of Energy, Office of Science, and Office of Biological and Environmental Research. The Advanced Light Source is supported by the Director, Office of Science, and Office of Basic Energy Sciences. Both were supported through Contract DE-AC02-05CH11231.

REFERENCES

(1) Lewis, E. N.; Treado, P. J.; Reeder, R. C.; Story, G. M.; Dowrey, A. E.; Marcott, C.; Levin, I. W. *Anal. Chem.* **1995**, *67*, 3377−3381.

(2) Holman, H.-Y.; Martin, M. C.; McKinney, W. R. *J. Biol. Phys.* **2003**, *29*, 275−286.

(3) Jamin, N.; Dumas, P.; Moncuit, J.; Fridman, W.-H.; Teillaud, J.-L.; Carr, G. L.; Williams, G. P. *Proc. Natl. Acad. Sci. U.S.A.* **1998**, *95*, 4837−4840.

(4) Lasch, P.; Boese, M.; Pacifico, A.; Diem, M. *Vib. Spectrosc.* **2002**, *28*, 147−157.

(5) Lasch, P.; Haensch, W.; Naumann, D.; Diem, M. *Biochim. Biophys. Acta, Mol. Basis Dis.* **2004**, *1688*, 176−186.

(6) Travo, A.; Piot, O.; Wolthuis, R.; Gobinet, C.; Manfait, M.; Bara, J.; Forgue-Lafitte, M.-E.; Jeannesson, P. *Histopathology* **2010**, *56*, 921−931.

DOI: 10.1021/acs.analchem.5b00524
Anal. Chem. 2015, 87, 4601−4606

(7) Holman, H.-Y. N.; Miles, R.; Hao, Z.; Wozei, E.; Anderson, L. M.; Yang, H. *Anal. Chem.* **2009**, *81*, 8564−8570.
(8) Holman, H.-Y. N.; Wozei, E.; Lin, Z.; Comolli, L. R.; Ball, D. A.; Borglin, S.; Fields, M. W.; Hazen, T. C.; Downing, K. H. *Proc. Natl. Acad. Sci. U.S.A.* **2009**, *106*, 12599−12604.
(9) Holman, H.-Y. N.; Bechtel, H. A.; Hao, Z.; Martin, M. C. *Anal. Chem.* **2010**, *82*, 8757−8765.
(10) Miller, L. M.; Bourassa, M. W.; Smith, R. J. *Biochim. Biophys. Acta, Biomembr.* **2013**, *1828*, 2339−2346.
(11) Birarda, G.; Bedolla, D. E.; Mitri, E.; Pacor, S.; Grenci, G.; Vaccari, L. *Analyst* **2014**, *139*, 3097−3106.
(12) Kuimova, M. K.; Chan, K.; Kazarian, S. G. *Appl. Spectrosc.* **2009**, *63*, 164−171.
(13) Flower, K. R.; Khalifa, I.; Bassan, P.; Démoulin, D.; Jackson, E.; Lockyer, N. P.; McGown, A. T.; Miles, P.; Vaccari, L.; Gardner, P. *Analyst* **2011**, *136*, 498−507.
(14) Heraud, P.; Ng, E. S.; Caine, S.; Yu, Q. C.; Hirst, C.; Mayberry, R.; Bruce, A.; Wood, B. R.; McNaughton, D.; Stanley, E. G.; Elefanty, A. G. *Stem Cell Res.* **2010**, *4*, 140−147.
(15) Chen, L.; Holman, H.-Y. N.; Hao, Z.; Bechtel, H. A.; Martin, M. C.; Wu, C.; Chu, S. *Anal. Chem.* **2012**, *84*, 4118−4125.
(16) Birarda, G.; Grenci, G.; Businaro, L.; Marmiroli, B.; Pacor, S.; Piccirilli, F.; Vaccari, L. *Vib. Spectrosc.* **2010**, *53*, 6−11.
(17) Moss, D. A.; Keese, M.; Pepperkok, R. *Vib. Spectrosc.* **2005**, *38*, 185−191.
(18) Heraud, P.; Wood, B. R.; Tobin, M. J.; Beardall, J.; McNaughton, D. *FEMS Microbiol. Lett.* **2005**, *249*, 219−225.
(19) Nasse, M.; Ratti, S.; Giordano, M.; Hirschmugl, C. *Appl. Spectrosc.* **2009**, *63*, 1181−1186.
(20) Birarda, G.; Grenci, G.; Businaro, L.; Marmiroli, B.; Pacor, S.; Vaccari, L. *Microelectron. Eng.* **2010**, *87*, 806−809.
(21) Tobin, M. J.; Puskar, L.; Barber, R. L.; Harvey, E. C.; Heraud, P.; Wood, B. R.; Bambery, K. R.; Dillon, C. T.; Munro, K. L. *Vib. Spectrosc.* **2010**, *53*, 34−38.
(22) Young, E. W.; Beebe, D. J. *Chem. Soc. Rev.* **2010**, *39*, 1036−1048.
(23) Kazarian, S. G.; Chan, K. A. *Analyst* **2013**, *138*, 1940−1951.
(24) Miller, L. M.; Dumas, P. *Biochim. Biophys. Acta, Biomembr.* **2006**, *1758*, 846−857.
(25) McGuire, J. C.; Greene, L. A.; Furano, A. V. *Cell* **1978**, *15*, 357−365.
(26) Vaudry, D.; Stork, P.; Lazarovici, P.; Eiden, L. *Science* **2002**, *296*, 1648−1649.
(27) Filik, J.; Frogley, M. D.; Pijanka, J. K.; Wehbe, K.; Cinque, G. *Analyst* **2012**, *137*, 853−861.
(28) Bassan, P.; Lee, J.; Sachdeva, A.; Pissardini, J.; Dorling, K. M.; Fletcher, J. S.; Henderson, A.; Gardner, P. *Analyst* **2013**, *138*, 144−157.
(29) Wrobel, T. P.; Wajnchold, B.; Byrne, H. J.; Baranska, M. *Vib. Spectrosc.* **2013**, *69*, 84−92.
(30) Wang, T. D.; Triadafilopoulos, G.; Crawford, J. M.; Dixon, L. R.; Bhandari, T.; Sahbaie, P.; Friedland, S.; Soetikno, R.; Contag, C. H. *Proc. Natl. Acad. Sci. U.S.A.* **2007**, *104*, 15864−15869.
(31) Cooke, R.; Kuntz, I. *Annu. Rev. Biophys. Bioeng.* **1974**, *3*, 95−126.
(32) Boat, T.; Cheng, P. W. *Fed. Proc.* **1980**, 3067−3074.
(33) Barth, A.; Zscherp, C. Q. *Rev. Biophys.* **2002**, *35*, 369−430.

DOI: 10.1021/acs.analchem.5b00524
Anal. Chem. 2015, 87, 4601−4606